

Semantic Consistency in Image-to-Image Translation for Unsupervised Domain Adaptation

Stephan Brehm¹, Sebastian Scherer¹ and Rainer Lienhart¹

¹*Department of Computer Science, University of Augsburg, Universitätsstr. 6a, Augsburg, Germany*
{stephan.brehm, sebastian.scherer, rainer.lienhart}@informatik.uni-augsburg.de

Keywords: Image Translation, Semi-Supervised Learning, Unsupervised Learning, Domain Adaption, Semantic Segmentation, Synthetic Data, Semantic Consistency, Generative Adversarial Networks

Abstract: Unsupervised Domain Adaptation (UDA) aims to adapt models trained on a source domain to a new target domain where no labelled data is available. In this work, we investigate the problem of UDA from a synthetic computer-generated domain to a similar but real-world domain for learning semantic segmentation. We propose a semantically consistent image-to-image translation method in combination with a consistency regularisation method for UDA. We overcome previous limitations on transferring synthetic images to real looking images. We leverage pseudo-labels in order to learn a generative image-to-image translation model that receives additional feedback from semantic labels on both domains. Our method outperforms state-of-the-art methods that combine image-to-image translation and semi-supervised learning on relevant domain adaption benchmarks, i.e., on GTA5 to Cityscapes and SYNTHIA to Cityscapes.

1 INTRODUCTION

The problem of domain adaption from a synthetic source domain to the real target domain is mainly motivated by the cheap and almost endless possibilities of automated creation of synthetic data. In contrast, data from the real domain is often hard to acquire. This is especially true for most types of labelled data. A common problem in computer vision, for which acquiring real labelled data is exceptionally hard, is semantic segmentation, because it requires annotations at the pixel level. Due to this, a reasonable approach is to learn as much as possible from synthetic data and then transfer the knowledge to the real domain. However, convolutional neural networks (CNNs), in general, learn features from the domain on which they are trained on. This causes networks to perform poorly on unseen domains due to the visual gap between these domains. Unsupervised domain adaptation (UDA) aims to bridge this domain gap in order to learn models that perform well in the target domain without ever using labels from that domain.

In this work, we aim to improve the quality and usefulness of synthetic data by transforming synthetic images such that they look more like real images. However, such an Image-to-Image Translation (I2I) approach cannot change fundamental differences in image content because it needs to keep the trans-

formed images consistent to the semantic labels of synthetic images. Because of this, we cannot bridge the gap between synthetic and real domains solely by an I2I approach. The remaining differences are in image content and include object shapes, object frequency, and differences in viewpoint. Following recent work, we utilise a self-training framework which allows us to include unlabelled data from the real target domain into the training of a semantic segmentation network. The main contributions of our work are summarised as follows:

1. We propose a semantically consistent I2I method that combines an adversarial approach with a segmentation objective that is optimised jointly by both generator and discriminator.
2. We improve both adversarial and segmentation objectives with self-supervised techniques that include the unlabelled data from the real target domain into the training. Our method outperforms state-of-the-art combinations of I2I and Semi-Supervised Learning (SSL) on challenging benchmarks for UDA. We provide extensive experiments and analyses and show which components are essential to our approach.

2 Related Work

Semantic Segmentation is the task of labelling every pixel of an image according to the object class it belongs to. In 2015, Long *et al.* proposed fully convolution neural networks (FCNs) (Long et al., 2015) improving massively upon classical methods for semantic segmentation. Since then, many new methods based on deep convolutional neural networks were proposed (Chen et al., 2017a; Wang et al., 2020b; Yu and Koltun, 2016). However, these methods are directly learned on the real target domain in a supervised fashion. In contrast, our method is able to learn about the real domain without the necessity of annotated real data.

Image-to-Image translation (I2I) methods (Choi et al., 2019; Pizzati et al., 2020) have been widely used to bridge the gap between synthetic and real data, i.e., these methods try to make the synthetic data look more real. Here, it is important to keep the overall image consistent with the synthetic labels.

Adversarial training is often used in UDA methods to adapt either input space, feature space or output space of a semantic segmentation network (Toldo et al., 2020). On the feature level, a discriminator is trained to distinguish between feature maps from different domains (Hoffman et al., 2016; Chen et al., 2017b; Hong et al., 2018). Popular input space adaptation techniques utilise frameworks based on cycle consistency (Zhu et al., 2017) for UDA (Hoffman et al., 2018; Sankaranarayanan et al., 2018; Chen et al., 2019; Murez et al., 2018). However, cycle consistency allows almost arbitrary transformations as long as they can be reversed. In contrast to these methods, we perform input space adaption in our I2I method without the need for cycle consistency. Our method simply uses the annotations of the synthetic data to directly enforce consistency.

Semi-supervised learning (SSL) aims to include unlabelled data into the training which allows to use data from the real domain. The dominant approaches for SSL are pseudo-labelling and consistency regularisation. An extensive overview can be found in this survey (van Engelen and Hoos, 2020). A common approach to SSL is Pseudo-Labeling. It was first proposed in (Lee, 2013). Xie *et al.* (Xie et al., 2019) recently showed that pseudo-labels can indeed improve overall performance on image classification tasks. They train a network on labelled data and reuse high-confidence predictions on unlabelled data as pseudo-labels. Pseudo-labels are then included in

the full dataset on which a new model is subsequently trained from scratch.

Many recent SSL methods (Ke et al., 2019; Tarvainen and Valpola, 2017) include consistency regularisation. They employ unlabelled data to produce consistent predictions under different perturbations. Possible perturbations can be data augmentation, dropout or simple noise on the input data. The trained model should be robust against such perturbations. These approaches leverage the idea that a classifier should output the same distribution for different augmented versions of an unlabelled sample. This is typically achieved by minimising the difference between the prediction of a model on different perturbed versions of the same input. We also utilise this approach to boost our performance further and use pseudo-labels for our I2I translation module.

3 Method

In this work, we assume that image data is available from both the synthetic *source* domain as well as the real *target* domain. However, annotations are only available in the synthetic *source* domain. We aim to bridge the gap between the *source* and the *target* data. The first step is to bring the two domains closer together visually which means transforming the synthetic data such that it looks more real. By keeping consistency with the labels of the synthetic source data, we are able to generate a dataset of images with corresponding labels that closely resembles the real target data in terms of colour, texture and lighting. Basically, we aim to improve domain adaptation by transferring the style of the real target domain onto images of the synthetic source domain. However, fundamental differences in image composition cannot be learned with such an I2I method. For this reason, we use the translated synthetic data in conjunction with unlabelled data from the real *target* domain to train our segmentation model. We propose a training process that consists of three phases.

- (a) In the *warm-up phase* the SSL method is used to train an initial segmentation model M_0 as the initial pseudo label generator.
- (b) In the *I2I training phase*, we use the pseudo labels from model M_0 and train our generator G to produce real looking images from synthetic images.
- (c) In the *segmentation training phase*, we combine the SSL method with the translated images by generator G and train our new segmentation network M_1 .

3.1 Notation

In the following, we will denote \mathcal{S} as the *source* domain and \mathcal{T} as the *target* domain. $X_{\mathcal{S}}$ and $X_{\mathcal{T}}$ are sets of images sampled from \mathcal{S} and \mathcal{T} , i.e., synthetic images and real images, respectively. $\mathbf{x}^s \in X_{\mathcal{S}}$ and $\mathbf{x}^t \in X_{\mathcal{T}}$ are images sampled from their respective image sets $X_{\mathcal{S}}$ and $X_{\mathcal{T}}$.

Both domains \mathcal{S} and \mathcal{T} share a common set of categories C . We denote the label of an image \mathbf{x}^d of domain $d \in \{\mathcal{S}, \mathcal{T}\}$ as \mathbf{y}^d . In this work \mathbf{y}^s generally is a synthetic segmentation mask and $\hat{\mathbf{y}}^t$ is a segmentation mask that contains pseudo-labels. $\mathcal{L}_{i,j,c}^{W,n}(\mathbf{x}, \mathbf{y})$ denotes a loss function based on image \mathbf{x} and label \mathbf{y} that is used to update trainable parameters of a network W . n is an identifier/name for the loss function. Note that we often omit the arguments (\mathbf{x}, \mathbf{y}) in order to simplify our notation. Also note that W only indicates which network is updated by \mathcal{L}^n and thus may also be omitted in more general statements and definitions. i, j, c are indices that we use to refer to specific dimensions and or individual values in the calculated loss if necessary. In general, we assume multidimensional arrays to be in the order of *height* \times *width* \times *channels*.

In this work, we aim to train a segmentation network $F_{\mathcal{S}}$ on $X_{\mathcal{S}}$ that generalises to $X_{\mathcal{T}}$.

3.2 Image-to-Image Translation

In order to generalise to a target domain \mathcal{T} we aim to move our source images $X_{\mathcal{S}}$ closer to \mathcal{T} . In this section, we detail our approach to this goal. Figure 1 illustrates the employed architecture. We aim to transfer images from a synthetic domain to the real domain, because the synthetic domain allows to easily create images and corresponding labels by simulating an environment that is similar to the real environment. The transformed images are supposed to deliver maximum performance on real data when learning a fully convolutional method for semantic segmentation. In order to achieve this, such a transformation needs to meet two major requirements.

1. Transformed images need to look as realistic as possible
2. Transformed images need to maintain consistency to the segmentation labels

We propose an I2I method that consists of two networks in an adversarial setting. Our learning task is designed to enforce the requirements given above. Requirement 1. is tackled by an adversarial objective. For Requirement 2, we extend the adversarial setting with an additional cooperative segmentation objective

that is jointly optimised by both adversaries. Following, we give a brief overview of the employed generator and discriminator architectures.

Generator We use a simple encoder-decoder architecture with strided convolutions for down-sampling the input image by a factor of 8. These down-sampling operations are followed by a single residual block. The decoder is simply a stack of deconvolution layers. Note that we do not include any skip/residual connections between encoder and decoder. In every layer, we append a learned scaling factor as well as a learned bias term. We use leaky-ReLU activations for all layers except the output layer. We also use deconvolution kernels, PixelNorm, Equalized Learning Rate, Adaptive Instance Normalization and Stochastic Variation as proposed in (Karras et al., 2018). Similar to Taigman *et al.* (Taigman et al., 2016), we incorporate images from the target domain in the training of the generator by adding an identity objective. Thus, the generator learns to encode and reconstruct real images in addition to its main I2I task. The additional feedback is a way to directly learn about the structure and texture of real images.

Discriminator Instead of discriminating between generated images and real images directly, we propose to use prior knowledge for discrimination. We use image-features of an ImageNet-pretrained(Deng et al., 2009) VGG16 network (Simonyan and Zisserman, 2015) after layer *block3_conv3*. We build additional 3 residual blocks (He et al., 2016) on top of these features. Note that we do not fine-tune the pre-trained VGG16 part of the discriminator. Our discriminator features two distinct outputs which are each computed on top of a separate decoder, as illustrated in Figure 1. We refer to these decoders as the GAN-head (Goodfellow et al., 2014) and the auxiliary classifier head (AC-head) (Odena et al., 2017). Both heads output results at image resolution. The task of the AC-head is to learn semantic segmentation in the target domain. Thus we feed the translated images in conjunction with the labels of the synthetic data as well as real images with corresponding pseudo-labels. Note that these pseudo-labels can be created online during training.

However, using pseudo-labels created by our proposed segmentation system that is detailed in section 3.3 generally improved results. The AC-head is important in two ways. First, the segmentation feedback generated in the AC-head forces previous layers to learn segmentation-specific features which in turn helps the GAN-head to discriminate between images that are translated from the synthetic domain and im-

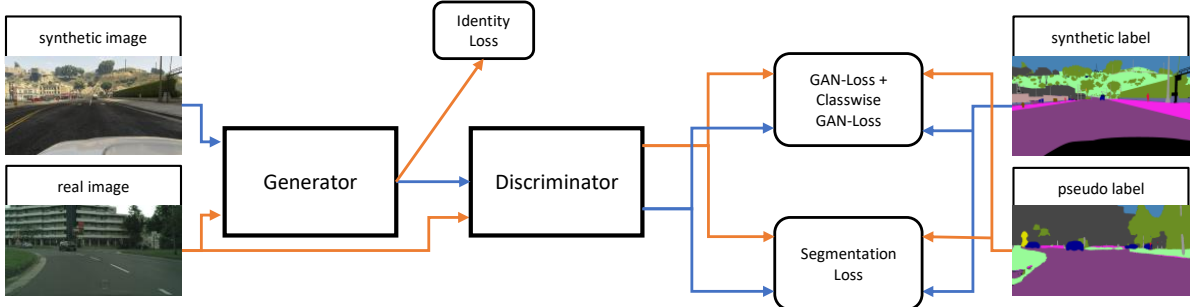


Figure 1: Schematic illustration of our proposed I2I method. The colored arrows visualize data-flow.

ages from the real domain. Second, it provides consistency feedback for the generator. We achieve this by propagating gradients based on the segmentation loss of the AC-head into the weights of the discriminator as well as into the weights of the generator. Thus effectively optimising a joint segmentation objective in both generator and discriminator. This way, the generator is punished if the translated images are not consistent with the label of the synthetic input data.

Note that GAN-Heads are commonly learned with a single label only (*real* or *fake*). We extend this formulation to include class information. Thus, allowing the discriminator to directly learn to compare images on a class specific level. We utilize segmentation labels in the GAN-head to create this class-specific feedback. In GAN-terminology this means that we treat pseudo-labels as real and the synthetic labels as fake. For each class, we produce an additional output feature map. On this feature map, feedback is only applied at positions that belong to the given object class as defined by either synthetic labels or pseudo-labels.

Optimisation Given the supervised segmentation loss $\mathcal{L}^{seg}(D(G(\mathbf{x}^s)), \mathbf{y}^s)$ (softmax cross-entropy) based on synthetic labels and the supervised segmentation loss $\mathcal{L}^{seg}(D(\mathbf{x}^t), \hat{\mathbf{y}}^t)$ based on the pseudo-labels, we compute the total segmentation loss \mathcal{L}^{seg} as given in Equation 1. We use symmetric cross-entropy loss (Wang et al., 2019) for $\mathcal{L}^{seg}(D(\mathbf{x}^t), \hat{\mathbf{y}}^t)$ because it increases robustness when using noisy pseudo-labels $\hat{\mathbf{y}}^t$.

$$\mathcal{L}^{seg} = \mathcal{L}^{seg}(D(G(\mathbf{x}^s)), \mathbf{y}^s) + \lambda^{pl} \mathcal{L}^{seg}(D(\mathbf{x}^t), \hat{\mathbf{y}}^t) \quad (1)$$

where λ^{pl} is a scaling factor that we use to control the relative impact of the pseudo-labels on the overall error of the model.

Like the segmentation loss, we calculate the GAN-Loss \mathcal{L}^{gan} on a pixel-wise basis, i.e., the GAN-loss is the average of all losses computed over all pixels $I_{i,j}$ of an input image I . Let $m(a, b)$ be a derivable distance metric between a and b . We give a general

error function $\mathcal{L}^{D,dgan}$ for a discriminator D as well as a general error function $\mathcal{L}^{G,dgan}$ for a generator G in Equation 2 and Equation 3 respectively.

$$\mathcal{L}_{i,j}^{D,dgan} = m(D(G(\mathbf{x}^s))_{i,j}, 0) + m(D(\mathbf{x}^t)_{i,j}, 1) \quad (2)$$

$$\mathcal{L}_{i,j}^{G,dgan} = m(D(G(\mathbf{x}^s))_{i,j}, 1) \quad (3)$$

We use the mean-squared error for the distance metric m .

Now let, \mathbf{y}^s be the one-hot encoded segmentation label for a given image \mathbf{x}^s , i.e., $\mathbf{y}_{i,j,c}^s$ equals one if $I_{i,j}$ belongs to class c . Otherwise $\mathbf{y}_{i,j,c}^s$ is zero. The same applies to the pseudo-label $\hat{\mathbf{y}}^t$. We define a class-wise and pixel-wise error $\mathcal{L}_{i,j,c}^{D,cgan}$ for discriminator D in Equation 4 and a class-wise and pixel-wise error $\mathcal{L}_{i,j,c}^{G,cgan}$ for generator G in Equation 5.

$$\begin{aligned} \mathcal{L}_{i,j,c}^{D,cgan} = & m(D(G(\mathbf{x}^s))_{i,j,c}, 0) \cdot \mathbf{y}_{i,j,c}^s + \\ & + m(D(\mathbf{x}^t)_{i,j,c}, 1) \cdot \hat{\mathbf{y}}_{i,j,c}^t \end{aligned} \quad (4)$$

$$\mathcal{L}_{i,j,c}^{G,cgan} = m(D(G(\mathbf{x}^s))_{i,j,c}, 1) \cdot \mathbf{y}_{i,j,c}^s \quad (5)$$

Hence, the full adversarial loss for D is:

$$\begin{aligned} \mathcal{L}^{D,gan} = & \\ & \sum_{i=0}^H \sum_{j=0}^W \left(\mathcal{L}_{i,j}^{D,dgan} + \frac{\lambda^{cgan}}{|C|} \sum_{c \in C} \mathcal{L}_{i,j,c}^{D,cgan} \right). \end{aligned} \quad (6)$$

where λ^{cgan} is a scaling factor that we use to control the relative impact of the class-wise loss on the overall error of the model, H is the height and W is the width of both images and labels. $\mathcal{L}^{G,gan}$ can be computed analogous.

The total loss of the discriminator \mathcal{L}^D is a combination of segmentation and GAN losses as given in Equation 7.

$$\mathcal{L}^D = \frac{1}{HW} (\mathcal{L}^{D,seg} + \mathcal{L}^{D,gan}) \quad (7)$$

With $\mathcal{L}^{G,id}$ being the identity reconstruction error on a real image \mathbf{x}^t from the target domain, we compute

the generator loss \mathcal{L}^G as given in Equation 9.

$$\mathcal{L}^{G,id} = \sum_{i=0}^H \sum_{j=0}^W \|G(\mathbf{x}^t)_{i,j} - \mathbf{x}^t_{i,j}\|_1 \quad (8)$$

$$\mathcal{L}^G = \frac{1}{HW} \left(\mathcal{L}^{G,seg} + \mathcal{L}^{G,gan} + \mathcal{L}^{G,id} \right) \quad (9)$$

Note that the second term of \mathcal{L}^{seg} from Equation 1 is not affected by G and thus $\mathcal{L}^{G,seg}$ is reduced to the first term of \mathcal{L}^{seg} when back-propagating. This means that G should generate images that match the synthetic segmentation labels. On the other hand, $\mathcal{L}^{G,gan}$ incentivises more realistic images. By using $\mathcal{L}^{G,id}$ we are able to show real images from the target domain to G . This combination of various objectives enables us to learn an I2I model that satisfies the requirement of realistic transformation while simultaneously keeping consistency with the synthetic labels. We use the resulting images to subsequently learn a better segmentation model.

3.3 Segmentation Training

At this point, we are able to transform synthetic images into real images while keeping the semantic content of the image unchanged. Thus, we can use the transformed images with the original synthetic annotations. However, some issues remain to be solved. The remaining differences are in image content and include object shapes, object frequency, and differences in viewpoint which can not be learned by our I2I module. As a solution, we incorporate images from the real domain directly into the training of the segmentation model via a SSL framework.

Similar to Tarvainen *et al.* (Tarvainen and Valpola, 2017), we make use of two networks: a student network F_S and a teacher network F_T . The architecture of the teacher network is identical to the one of the student network. The weights of the teacher model are an Exponential Moving Average (EMA) of the student’s weights. Given an image from the target domain, the teacher’s prediction serves as a label for the student, forcing consistency in the prediction of both models under different perturbations.

The overall objective \mathcal{L}^{F_S} is a combination of a supervised segmentation loss $\mathcal{L}^{F_S,seg}$ and the self-supervised consistency loss $\mathcal{L}^{F_S,con}$ as detailed in Equation 10.

$$\mathcal{L}^{F_S} = \mathcal{L}^{F_S,seg}(\mathbf{x}^s, \mathbf{y}^s) + \lambda^{con} \mathcal{L}^{F_S,con}(\mathbf{x}^t), \quad (10)$$

where λ^{con} is a trade-off parameter.

For the supervised training, we incorporate synthetic images $\mathbf{x}^s \in X_S$ and a transformed version obtained from the generator $G(\mathbf{x}^s)$ of our proposed I2I

method. We calculate a combined loss $\mathcal{L}^{F_S,seg}$ as given in Equation 11

$$\mathcal{L}^{F_S,seg} = \mathcal{L}^{seg}((F_S(\mathbf{x}^s)), \mathbf{y}^s) + \mathcal{L}^{seg}((F_S(G(\mathbf{x}^s))), \mathbf{y}^s), \quad (11)$$

where \mathcal{L}^{seg} again is the softmax cross-entropy error.

For the semi-supervised training, we incorporate images from the real domain $\mathbf{x}^t \in X_T$. We calculate the consistency loss $\mathcal{L}^{F_S,con}(\mathbf{x}^t)$ as given in Equation 12.

$$\mathcal{L}^{F_S,con} = \|\sigma(F_T(\mathbf{x}^t)) - \sigma(F_S(\mathbf{P}(\mathbf{x}^t)))\|_2^2, \quad (12)$$

where σ is the softmax activation function and $\mathbf{P}(\mathbf{x}^t)$ is a strongly perturbed version of the input image \mathbf{x}^t . Similar to (Zhou et al., 2020), we utilise color jittering, Gaussian blurring and noise as perturbations on \mathbf{x}^t .

As our I2I model needs pseudo-labels, we perform an identical training with supervised and consistency loss, but without transformed images $G(\mathbf{x}^s)$. We use the resulting model to generate pseudo-labels that we use to train G .

4 Experiments and Results

In this section, we detail experiments that we conducted in order to show the performance of our proposed methods. In Section 4.1 we shortly introduce the datasets that we used. In Section 4.2 we give important details on the training and validation protocols. In Section 4.3 we compare our methods to previous state-of-the art methods on two public benchmarks. In Section 4.4 we conduct an ablation study to show the impact of individual components on our results.

4.1 Datasets

Following common practice for unsupervised domain adaption in semantic segmentation, we use the GTA5 (Richter et al., 2016) and SYNTHIA (Ros et al., 2016) datasets as our synthetic domain and the Cityscapes dataset (Cordts et al., 2016) as our real domain. The datasets are detailed below.

Cityscapes dataset (Cordts et al., 2016) contains images of urban street scenes collected around Germany and neighbouring countries. It consists of a training set with 2975 images and a validation set of 500 images. Another 89250 unlabeled images of additional frames are available for training.

Table 1: Results of domain adaption from GTA5 to Cityscapes. All methods use a VGG16 backbone.

	road	sidewalk	building	wall	fence	pole	traffic light	traffic sign	vegetation	terrain	sky	person	rider	car	truck	bus	train	motorbike	bicycle	mIoU
Source only (ours)	79.2	30.6	76.0	22.7	11.1	19.2	11.0	2.2	80.3	30.4	73.5	39.3	0.5	75.3	17.3	9.5	0.0	1.4	0.0	30.5
CyCADA (Hoffman et al., 2018)	85.2	37.2	76.5	21.8	15.0	23.8	22.9	21.5	80.5	31.3	60.7	50.5	9.0	76.9	17.1	28.2	4.5	9.8	0.0	35.4
CBST-SP (Zou et al., 2018)	90.4	50.8	72.0	18.3	9.5	27.2	28.6	14.1	82.4	25.1	70.8	42.6	14.5	76.9	5.9	12.5	1.2	14.0	28.6	36.1
DCAN (Wu et al., 2018)	82.3	26.7	77.4	23.7	20.5	20.4	30.3	15.9	80.9	25.4	69.5	52.6	11.1	79.6	24.9	21.2	1.3	17.0	6.7	36.2
SWD (Lee et al., 2019)	91.0	35.7	78.0	21.6	21.7	31.8	30.2	25.2	80.2	23.9	74.1	53.1	15.8	79.3	22.1	26.5	1.5	17.2	30.4	39.9
SIM (Wang et al., 2020c)	88.1	35.8	83.1	25.8	23.9	29.2	28.8	28.6	83.0	36.7	82.3	53.7	22.8	82.3	26.4	38.6	0.0	19.6	17.1	42.4
TGCF-DA + SE (Choi et al., 2019)	90.2	51.5	81.1	15.0	10.7	37.5	35.2	28.9	84.1	32.7	75.9	62.7	19.9	82.6	22.9	28.3	0.0	23.0	25.4	42.5
FADA (Wang et al., 2020a)	92.3	51.1	83.7	33.1	29.1	28.5	28.0	21.0	82.6	32.6	85.3	55.2	28.8	83.5	24.4	37.4	0.0	21.1	15.2	43.8
PCEDA (Yang et al., 2020)	90.2	44.7	82.0	28.4	28.4	24.4	33.7	35.6	83.7	40.5	75.1	54.4	28.2	80.3	23.8	39.4	0.0	22.8	30.8	44.6
Zhou et al. (Zhou et al., 2020)	95.1	66.5	84.7	35.1	19.8	31.2	35.0	32.1	86.2	43.4	82.5	61.0	25.1	87.1	35.3	46.1	0.0	24.6	17.5	47.8
Ours	94.4	65.3	85.9	39.0	22.2	35.4	39.1	37.3	86.7	42.3	88.1	62.7	36.2	87.6	33.8	45.0	0.0	26.5	24.2	50.1
Target only (ours)	96.9	79.7	89.6	46.0	47.6	47.4	55.9	64.5	90.0	60.7	91.7	72.4	49.1	92.4	56.7	75.4	54.0	51.0	69.4	68.0

Table 2: Results of domain adaption from SYNTHIA to Cityscapes. All methods use a VGG16 backbone. mIoU and mIoU* are computed on 16 and 13 classes respectively (* excluded).

	road	sidewalk	building	wall*	fence*	pole*	traffic light	traffic sign	vegetation	sky	person	rider	car	bus	motorbike	bicycle	mIoU	mIoU*
Source only (ours)	42.0	19.6	60.4	6.3	0.1	28.3	2.1	10.3	76.2	76.0	44.3	7.2	62.5	14.8	3.2	10.6	29.0	33.0
DCAN (Wu et al., 2018)	79.9	30.4	70.8	1.6	0.6	22.3	6.7	23.0	76.9	73.9	41.9	16.7	61.7	11.5	10.3	38.6	35.4	-
CBST (Zou et al., 2018)	69.6	28.7	69.5	12.1	0.1	25.4	11.9	13.6	82.0	81.9	49.1	14.5	66.0	6.6	3.7	32.4	35.4	40.7
SWD (Lee et al., 2019)	83.3	35.4	82.1	-	-	-	12.2	12.6	83.8	76.5	47.4	12.0	71.5	17.9	1.6	29.7	-	43.5
FADA (Wang et al., 2020a)	80.4	35.9	80.9	2.5	0.3	30.4	7.9	22.3	81.8	83.6	48.9	16.8	77.7	31.1	13.5	17.9	39.5	46.0
TGCF-DA + SE (Choi et al., 2019)	90.1	48.6	80.7	2.2	0.2	27.2	3.2	14.3	82.1	78.4	54.4	16.4	82.5	12.3	1.7	21.8	38.5	46.6
PCEDA (Yang et al., 2020)	79.7	35.2	78.7	1.4	0.6	23.1	10.0	28.9	79.6	81.2	51.2	25.1	72.2	24.1	16.7	50.4	41.1	48.7
Zhou et al. (Zhou et al., 2020)	93.1	53.2	81.1	2.6	0.6	29.1	7.8	15.7	81.7	81.6	53.6	20.1	82.7	22.9	7.7	31.3	41.5	48.6
Ours	94.8	67.2	81.9	6.1	0.1	29.6	0.1	19.7	82.2	81.1	50.2	17.0	84.6	30.8	12.4	25.1	42.7	49.8
Target only (ours)	96.9	79.7	89.6	46.0	47.6	47.4	55.9	64.5	90.0	91.7	72.4	49.1	92.4	75.4	51.0	69.4	70.0	75.4

Table 3: Ablation study and comparison to existing similar work. We evaluate and compare the image translation and constancy regularization. We report results from GTA5 to Cityscapes. $\mathcal{L}_{S,seg}$ is the segmentation loss defined in Equation 11 and $\mathcal{L}_{S,con}$ is the consistency loss from Equation 12. IT means that we use translated images from the proposed I2I method.

Method	Component	mIoU
Source Only	$\mathcal{L}_{S,seg}$	28.3
(Choi et al., 2019)	$\mathcal{L}_{S,seg} + \mathcal{L}_{S,con}$	32.6
(Zhou et al., 2020)	$\mathcal{L}_{S,seg} + \mathcal{L}_{S,con}$	35.6
Ours	$\mathcal{L}_{S,seg} + \mathcal{L}_{S,con}$	39.2
(Choi et al., 2019)	$\mathcal{L}_{S,seg} + IT$	35.4
(Zhou et al., 2020)	$\mathcal{L}_{S,seg} + IT$	35.1
Ours	$\mathcal{L}_{S,seg} + IT$	43.9
(Choi et al., 2019)	$\mathcal{L}_{S,seg} + \mathcal{L}_{S,con} + IT$	42.5
(Zhou et al., 2020)	$\mathcal{L}_{S,seg} + \mathcal{L}_{S,con} + IT$	47.8
Ours	$\mathcal{L}_{S,seg} + \mathcal{L}_{S,con} + IT$	50.1

GTA5 dataset (Richter et al., 2016) contains images rendered by the game Grand Theft Auto 5. It consists of 24966 images with corresponding pixel-level semantic segmentation annotations and a set of object classes that is compatible to the annotations of the Cityscapes dataset.

SYNTHIA dataset (Ros et al., 2016) consists of a collection of images rendered from a virtual city. We use the SYNTHIA-RAND-CITYSCAPES subset, which consists of 9400 images with pixel-wise annotations. We use the 16 classes that are common with the Cityscapes dataset.

4.2 Implementation details

For a fair comparison to earlier works (Choi et al., 2019; Zhou et al., 2020), we adopt the VGG16 backbone (Simonyan and Zisserman, 2015) pre-trained on the ImageNet dataset (Deng et al., 2009). Following Deeplab-v2 (Chen et al., 2017a), we incorporate Atrous Spatial Pyramid Pooling (ASPP) as the decoder and then use an bi-linear up-sampling layer to get the segmentation output. We use this model for all our experiments if not stated otherwise. We use the Adam optimiser (Kingma and Ba, 2015) for the segmentation training with an initial learning rate of 1×10^{-5} and exponential weight decay. The generator and discriminator are trained with a constant learning rate of 1×10^{-5} for 1 million iterations. For validation purposes, we keep exponential moving averages of the generator weights. We use a 50/50 split of synthetic and transformed data to learn the segmen-

tation model. All networks are trained with gradient clipping at a global norm of 5. We set all EMA decay values to 0.999. During the first 10,000 training steps of F_S , we keep λ^{con} to zero. We report results from the teacher network after the training, which is a smoothed version of the trained segmentation network. We fade λ^{pseudo} and λ^{cgan} linearly from zero at iteration 20,000 to 0.3 at iteration 100,000 when learning with pseudo-labels created online. When learning with pre-computed pseudo-labels from our proposed segmentation model, we keep λ^{pseudo} and λ^{cgan} at 0.3 at all times. All experiments are conducted at half of the original image resolution.

4.3 Comparisons with the State-of-the-Art

We compare the results of our method to state-of-the-art methods that combine I2I and SSL on the two standard benchmarks: “GTA5 to Cityscapes” and “SYNTHIA to Cityscapes” in Table 1 and Table 2, respectively. In case of training on the GTA5 dataset, it can be seen that our approach improves upon current state-of-the art. We provide further insights into the building blocks that have led to this improvement in the following section. It can be seen that our method outperforms existing state-of-the art methods in both benchmarks.

4.4 Ablation Study

In this section, we conduct an ablation study on various components of our proposed method. In addition, we compare different components directly to their counterparts in similar methods (Choi et al., 2019; Zhou et al., 2020). We also analyze the remaining domain gap to get a better understanding of our results.

Image-to-Image Translation. The results of the ablation study are shown in Table 5. For simplicity, we omit the SSL part of the third stage of our method, i.e., we use the images from our I2I method to learn a segmentation model in a purely supervised fashion. We train on 50% source data and 50% translated data. As expected, our performance is highly dependent on the semantic consistency loss $\mathcal{L}^{G,seg}$ from Equation 9 that we use to supervise the generator. We lose $\approx 5.7\%$ mIoU absolute performance by removing this component which demonstrates the effectiveness of our approach. Note that this ablation evaluates the impact of $\mathcal{L}^{G,seg}$. $\mathcal{L}^{D,seg}$ is still applied during training, i.e., the discriminator has access to the segmentation

information but is not able to properly transfer this information to the generator. This can be improved by applying $\mathcal{L}^{G,seg}$ during training which explicitly enforces the transfer of segmentation knowledge. Note that our method is still able to deliver 40% mIoU when using simple pseudo-labels created online during training from the output of the AC-head, i.e., if we train without pseudo-labels supplied by an external method. Nevertheless, using higher quality pseudo-labels from the proposed segmentation method increases performance by an absolute 3.8% mIoU. Removing the class-wise GAN feedback reduces performance by around 1.2% mIoU. Swapping the LSGAN target to a standard GAN (SGAN) target reduces performance by $\approx 1\%$ mIoU.

Figure 2 shows examples of transformed synthetic images. We observe that the textures of roads and trees look much more realistic. Also, the sky is generally more cloudy which is very characteristic for the Cityscapes dataset.

Comparison with similar methods. In Table 3, we compare our two main components to the main components of similar work by Choi *et al.* (Choi et al., 2019) and Zhou *et al.* (Zhou et al., 2020). We compare the components in isolation and in combination. Our I2I module is a substantial improvement upon previous work. As illustrated in Table 5, the improvement is predominantly achieved through the semantic consistency framework.

In order to estimate the remaining domain gap we retrain the linear classification layer on real labels from the Cityscapes dataset. We compare to a model that is trained on Cityscapes only. The results are summarized at Table 4. We argue that retraining the classification layer is needed for a proper comparison because it allows to overcome fundamental differences in class annotations between the synthetic source and the real target data. Also, we think that a supervised model gives a reasonable upper bound on the achievable segmentation performance. Our re-trained model achieves 59.0% mIoU while the model trained on real data achieves 68.0% mIoU. Thus, we estimate the remaining domain gap to be $\approx 9\%$. In Table 4 we also compare to a model that is purely trained on synthetic source data. Again, we retrain only the linear classification layer. This model achieves 39.6% mIoU. Thus, we can conclude that our method reduces the domain gap by 68.3%.

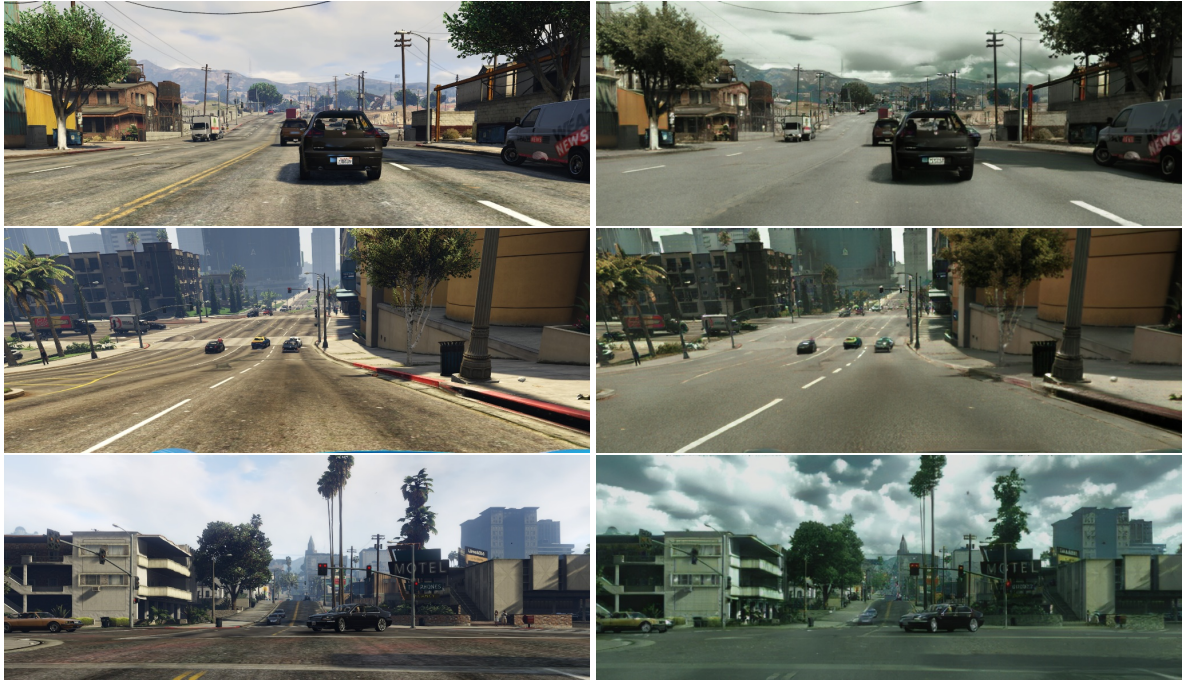


Figure 2: Examples of translated images. The left column shows synthetic images from the GTA5 dataset. The right column shows the corresponding translated images.

Table 4: Upper bound evaluation. Our method closes the domain gap between GTA5 and Cityscapes by 68.3%.

Method	mIoU	domain gap
Cityscapes Model	68.0	0.0%
Source only	39.6	100.0%
Ours	59.0	31.7%

Table 5: Ablation study for the proposed image-to-image translation method from the synthetic GTA5 to the Cityscapes dataset. We report mean Intersection over Union scores on the Cityscapes validation set.

Component	mIoU
LSGAN (Mao et al., 2017)	43.9
SGAN (Goodfellow et al., 2014)	42.9
w/o $\mathcal{L}^{D,G,clsgan}$	42.7
w/o $\mathcal{L}^{G,seg}$	38.1
w/o pre-computed pseudo-labels	40.0

5 Conclusion

In this work, we have investigated the problem of unsupervised domain adaption for semantic segmentation. We proposed two complementary approaches in order to reduce the gap between the data of the synthetic source domain and the real-world target domain. More specifically, we have shown that an image-to-image translation model that is trained with an additional segmentation task on images of both domains yields significantly better results. We show that

using pseudo-labels can be leveraged to improve this process. In addition, we have proposed a balancing scheme that effectively controls the relative importance of a supervised objective and a self-supervised objective during segmentation training. The combination of the proposed methods outperforms previous state-of-the-art combinations of image-to-image translation and semi-supervised learning for domain adaption on relevant benchmarks by a considerable margin.

REFERENCES

Chen, L.-C., Papandreou, G., Kokkinos, I., Murphy, K., and Yuille, A. L. (2017a). Deeplab: Semantic image segmentation with deep convolutional nets, atrous convolution, and fully connected crfs. *IEEE transactions on pattern analysis and machine intelligence*, 40(4):834–848. 2, 6

Chen, Y.-C., Lin, Y.-Y., Yang, M.-H., and Huang, J.-B. (2019). Crdoco: Pixel-level domain transfer with cross-domain consistency. In *Proceedings of the IEEE/CVF Conference on Computer Vision and Pattern Recognition*, pages 1791–1800. 2

Chen, Y.-H., Chen, W.-Y., Chen, Y.-T., Tsai, B.-C., Frank Wang, Y.-C., and Sun, M. (2017b). No more discrimination: Cross city adaptation of road scene segmenters. In *Proceedings of the IEEE International Conference on Computer Vision*, pages 1992–2001. 2

Choi, J., Kim, T., and Kim, C. (2019). Self-ensembling

with gan-based data augmentation for domain adaptation in semantic segmentation. In *Proceedings of the IEEE/CVF International Conference on Computer Vision*, pages 6830–6840. 2, 6, 7

Cordts, M., Omran, M., Ramos, S., Rehfeld, T., Enzweiler, M., Benenson, R., Franke, U., Roth, S., and Schiele, B. (2016). The cityscapes dataset for semantic urban scene understanding. In *Proc. of the IEEE Conference on Computer Vision and Pattern Recognition (CVPR)*. 5

Deng, J., Dong, W., Socher, R., Li, L.-J., Li, K., and Fei-Fei, L. (2009). Imagenet: A large-scale hierarchical image database. In *2009 IEEE conference on computer vision and pattern recognition*, pages 248–255. Ieee. 3, 6

Goodfellow, I., Pouget-Abadie, J., Mirza, M., Xu, B., Warde-Farley, D., Ozair, S., Courville, A., and Bengio, Y. (2014). Generative adversarial nets. In Ghahramani, Z., Welling, M., Cortes, C., Lawrence, N., and Weinberger, K. Q., editors, *Advances in Neural Information Processing Systems*, volume 27. Curran Associates, Inc. 3, 8

He, K., Zhang, X., Ren, S., and Sun, J. (2016). Deep residual learning for image recognition. In *Proceedings of the IEEE conference on computer vision and pattern recognition*, pages 770–778. 3

Hoffman, J., Tzeng, E., Park, T., Zhu, J.-Y., Isola, P., Saenko, K., Efros, A., and Darrell, T. (2018). Cycada: Cycle-consistent adversarial domain adaptation. In *International conference on machine learning*, pages 1989–1998. PMLR. 2, 6

Hoffman, J., Wang, D., Yu, F., and Darrell, T. (2016). Fcn in the wild: Pixel-level adversarial and constraint-based adaptation. *arXiv preprint arXiv:1612.02649*. 2

Hong, W., Wang, Z., Yang, M., and Yuan, J. (2018). Conditional generative adversarial network for structured domain adaptation. In *Proceedings of the IEEE Conference on Computer Vision and Pattern Recognition*, pages 1335–1344. 2

Karras, T., Aila, T., Laine, S., and Lehtinen, J. (2018). Progressive growing of gans for improved quality, stability, and variation. 3

Ke, Z., Wang, D., Yan, Q., Ren, J., and Lau, R. W. (2019). Dual student: Breaking the limits of the teacher in semi-supervised learning. In *Proceedings of the IEEE/CVF International Conference on Computer Vision*, pages 6728–6736. 2

Kingma, D. P. and Ba, J. (2015). Adam: A method for stochastic optimization. In Bengio, Y. and LeCun, Y., editors, *3rd International Conference on Learning Representations, ICLR 2015, San Diego, CA, USA, May 7-9, 2015, Conference Track Proceedings*. 6

Lee, C.-Y., Batra, T., Baig, M. H., and Ulbricht, D. (2019). Sliced wasserstein discrepancy for unsupervised domain adaptation. In *Proceedings of the IEEE/CVF Conference on Computer Vision and Pattern Recognition*, pages 10285–10295. 6

Lee, D.-H. (2013). Pseudo-label : The simple and efficient semi-supervised learning method for deep neural networks. *ICML 2013 Workshop : Challenges in Representation Learning (WREPL)*. 2

Long, J., Shelhamer, E., and Darrell, T. (2015). Fully convolutional networks for semantic segmentation. In *Proceedings of the IEEE conference on computer vision and pattern recognition*, pages 3431–3440. 2

Mao, X., Li, Q., Xie, H., Lau, R. Y., Wang, Z., and Paul Smolley, S. (2017). Least squares generative adversarial networks. In *Proceedings of the IEEE international conference on computer vision*, pages 2794–2802. 8

Murez, Z., Kolouri, S., Kriegman, D., Ramamoorthi, R., and Kim, K. (2018). Image to image translation for domain adaptation. In *Proceedings of the IEEE Conference on Computer Vision and Pattern Recognition*, pages 4500–4509. 2

Odena, A., Olah, C., and Shlens, J. (2017). Conditional image synthesis with auxiliary classifier gans. In *International conference on machine learning*, pages 2642–2651. PMLR. 3

Pizzati, F., Charette, R. d., Zaccaria, M., and Cerri, P. (2020). Domain bridge for unpaired image-to-image translation and unsupervised domain adaptation. In *Proceedings of the IEEE/CVF Winter Conference on Applications of Computer Vision*, pages 2990–2998. 2

Richter, S. R., Vineet, V., Roth, S., and Koltun, V. (2016). Playing for data: Ground truth from computer games. In Leibe, B., Matas, J., Sebe, N., and Welling, M., editors, *European Conference on Computer Vision (ECCV)*, volume 9906 of *LNCS*, pages 102–118. Springer International Publishing. 5, 6

Ros, G., Sellart, L., Materzynska, J., Vazquez, D., and Lopez, A. M. (2016). The synthia dataset: A large collection of synthetic images for semantic segmentation of urban scenes. In *Proceedings of the IEEE conference on computer vision and pattern recognition*, pages 3234–3243. 5, 6

Sankaranarayanan, S., Balaji, Y., Jain, A., Lim, S. N., and Chellappa, R. (2018). Learning from synthetic data: Addressing domain shift for semantic segmentation. In *Proceedings of the IEEE Conference on Computer Vision and Pattern Recognition*, pages 3752–3761. 2

Simonyan, K. and Zisserman, A. (2015). Very deep convolutional networks for large-scale image recognition. In Bengio, Y. and LeCun, Y., editors, *3rd International Conference on Learning Representations, ICLR 2015, San Diego, CA, USA, May 7-9, 2015, Conference Track Proceedings*. 3, 6

Taigman, Y., Polyak, A., and Wolf, L. (2016). Unsupervised cross-domain image generation. *arXiv preprint arXiv:1611.02200*. 3

Tarvainen, A. and Valpola, H. (2017). Mean teachers are better role models: Weight-averaged consistency targets improve semi-supervised deep learning results. In Guyon, I., Luxburg, U. V., Bengio, S., Wallach, H., Fergus, R., Vishwanathan, S., and Garnett, R., editors, *Advances in Neural Information Processing Systems*, volume 30. Curran Associates, Inc. 2, 5

Toldo, M., Maracani, A., Michieli, U., and Zanuttigh, P.

(2020). Unsupervised domain adaptation in semantic segmentation: a review. *Technologies*, 8(2):35. 2

van Engelen, J. E. and Hoos, H. H. (2020). A survey on semi-supervised learning. *Machine Learning*, 109(2):373–440. 2

Wang, H., Shen, T., Zhang, W., Duan, L.-Y., and Mei, T. (2020a). Classes matter: A fine-grained adversarial approach to cross-domain semantic segmentation. In *European Conference on Computer Vision*, pages 642–659. Springer. 6

Wang, J., Sun, K., Cheng, T., Jiang, B., Deng, C., Zhao, Y., Liu, D., Mu, Y., Tan, M., Wang, X., et al. (2020b). Deep high-resolution representation learning for visual recognition. *IEEE transactions on pattern analysis and machine intelligence*. 2

Wang, Y., Ma, X., Chen, Z., Luo, Y., Yi, J., and Bailey, J. (2019). Symmetric cross entropy for robust learning with noisy labels. In *Proceedings of the IEEE/CVF International Conference on Computer Vision*, pages 322–330. 4

Wang, Z., Yu, M., Wei, Y., Feris, R., Xiong, J., Hwu, W.-m., Huang, T. S., and Shi, H. (2020c). Differential treatment for stuff and things: A simple unsupervised domain adaptation method for semantic segmentation. In *Proceedings of the IEEE/CVF Conference on Computer Vision and Pattern Recognition (CVPR)*. 6

Wu, Z., Han, X., Lin, Y.-L., Uzunbas, M. G., Goldstein, T., Lim, S. N., and Davis, L. S. (2018). Dcan: Dual channel-wise alignment networks for unsupervised scene adaptation. In *Proceedings of the European Conference on Computer Vision (ECCV)*, pages 518–534. 6

Xie, Q., Hovy, E. H., Luong, M., and Le, Q. V. (2019). Self-training with noisy student improves imagenet classification. *CoRR*, abs/1911.04252. 2

Yang, Y., Lao, D., Sundaramoorthi, G., and Soatto, S. (2020). Phase consistent ecological domain adaptation. In *Proceedings of the IEEE/CVF Conference on Computer Vision and Pattern Recognition*, pages 9011–9020. 6

Yu, F. and Koltun, V. (2016). Multi-scale context aggregation by dilated convolutions. *International Conference on Learning Representations*. 2

Zhou, Q., Feng, Z., Cheng, G., Tan, X., Shi, J., and Ma, L. (2020). Uncertainty-aware consistency regularization for cross-domain semantic segmentation. *arXiv preprint arXiv:2004.08878*. 5, 6, 7

Zhu, J.-Y., Park, T., Isola, P., and Efros, A. A. (2017). Unpaired image-to-image translation using cycle-consistent adversarial networks. In *Proceedings of the IEEE International Conference on Computer Vision (ICCV)*. 2

Zou, Y., Yu, Z., Kumar, B., and Wang, J. (2018). Unsupervised domain adaptation for semantic segmentation via class-balanced self-training. In *Proceedings of the European conference on computer vision (ECCV)*, pages 289–305. 6